ARTICLE IN PRESS
+ MODEL
Acta Pharmaceutica Sinica B xxxx;xxx(xxx):xxx

Chinese Pharmaceutical Association
Institute of Materia Medica, Chinese Academy of Medical Sciences

Acta Pharmaceutica Sinica B

www.elsevier.com/locate/apsb
www.sciencedirect.com

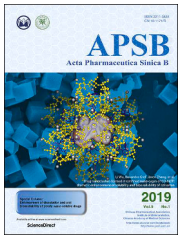

ORIGINAL ARTICLE

Yeast-two-hybrid based high-throughput screening to discover SARS-CoV-2 fusion inhibitors by targeting the HR1/HR2 interaction

Jing Zhang[a,†], Dongsheng Li[a,b,†], Wenwen Zhou[a,†], Chao Liu[a,†], Peirong Wang[c], Baoqing You[a], Bingjie Su[a], Keyu Guo[a], Wenjing Shi[a], Tin Mong Timothy Yung[c], Richard Yi Tsun Kao[c,*], Peng Gao[d,*], Yan Li[a,*], Shuyi Si[a,*]

[a]*State Key Laboratory of Bioactive Substances and Functions of Natural Medicines, Institute of Medicinal Biotechnology, Chinese Academy of Medical Sciences & Peking Union Medical College, Beijing, 100050, China*
[b]*Research Team of Molecular Medicine, The First Clinical Medical School of Shanxi Medical University, Taiyuan, 030001, China*
[c]*Department of Microbiology, Li Ka Shing Faculty of Medicine, The University of Hong Kong, Pok Fu Lam, Hong Kong SAR, China*
[d]*Applied Oral Sciences & Community Dental Care, Faculty of Dentistry, The University of Hong Kong, Pok Fu Lam, Hong Kong SAR, China*

Received 15 November 2024; received in revised form 27 February 2025; accepted 4 June 2025

KEY WORDS

SARS-CoV-2;
HR1/HR2 interaction;
Yeast-two-hybrid;
High-throughput screening;
IMB-9C;
Fusion inhibitor;
COVID-19;
Variants

Abstract The continuous emergence of SARS-CoV-2 variants as well as other potential future coronavirus has challenged the effectiveness of current COVID-19 vaccines. Therefore, there remains a need for alternative antivirals that target processes less susceptible to mutations, such as the formation of six-helix bundle (6-HB) during the viral fusion step of host cell entry. In this study, a novel high-throughput screening (HTS) assay employing a yeast-two-hybrid (Y2H) system was established to identify inhibitors of HR1/HR2 interaction. The compound IMB-9C, which achieved single-digit micromolar inhibition of SARS-CoV-2 and its Omicron variants with low cytotoxicity, was selected. IMB-9C effectively blocks the HR1/HR2 interaction *in vitro* and inhibits SARS-CoV-2-S-mediated cell−cell fusion. It binds to both HR1 and HR2 through non-covalent interaction and influences the secondary structure of HR1/HR2 complex. In addition, virtual docking and site-mutagenesis results suggest that amino acid residues A930,

*Corresponding authors.
E-mail addresses: sisy@imb.pumc.edu.cn (Shuyi Si), liyan@imb.pumc.edu.cn (Yan Li), gaopeng@hku.hk (Peng Gao), rytkao@hku.hk (Richard Yi Tsun Kao).
[†]These authors made equal contributions to this work.
Peer review under the responsibility of Chinese Pharmaceutical Association and Institute of Materia Medica, Chinese Academy of Medical Sciences.

https://doi.org/10.1016/j.apsb.2025.06.029
2211-3835 © 2025 The Authors. Published by Elsevier B.V. on behalf of Chinese Pharmaceutical Association and Institute of Materia Medica, Chinese Academy of Medical Sciences. This is an open access article under the CC BY-NC-ND license (http://creativecommons.org/licenses/by-nc-nd/4.0/).

Please cite this article as: Zhang Jing et al., Yeast-two-hybrid based high-throughput screening to discover SARS-CoV-2 fusion inhibitors by targeting the HR1/HR2 interaction, Acta Pharmaceutica Sinica B, https://doi.org/10.1016/j.apsb.2025.06.029

I931, K933, T941, and L945 are critical for IMB-9C binding to HR1. Collectively, in this study, we have developed a novel screening method for HR1/HR2 interaction inhibitors and identified IMB-9C as a potential antiviral small molecule against COVID-19 and its variants.

© 2025 The Authors. Published by Elsevier B.V. on behalf of Chinese Pharmaceutical Association and Institute of Materia Medica, Chinese Academy of Medical Sciences. This is an open access article under the CC BY-NC-ND license (http://creativecommons.org/licenses/by-nc-nd/4.0/).

1. Introduction

Three zoonotic coronaviruses (CoVs) are known to have caused outbreaks of fatal pneumonia in humans and posed serious threats to public health so far[1]. Severe acute respiratory syndrome (SARS) caused by SARS-CoV broke out in 2002 and spread to five continents[2,3]. Middle East respiratory syndrome (MERS) caused by MERS-CoV appeared in 2012 with a high fatality rate[4,5]. The coronavirus disease 2019 (COVID-19) caused by the severe acute respiratory syndrome coronavirus 2 (SARS-CoV-2) led to a global pandemic. Although the COVID-19 pandemic has been under control, expansion of new infectious diseases caused by different CoVs are of concern. Therefore, the discovery of additional effective antiviral drugs remains important[6].

The life cycle of viruses can be divided into several stages: attachment, entry, replication, maturation and release. Inhibiting the early stages of virus replication, such as attachment, viral envelope glycoprotein or fusion, has been an important strategy in the development of antivirals drugs[7-9]. By preventing the virus from entering host cells, these antivirals effectively block the initial stages of infection, reducing viral load and spread. This early intervention can limit the severity of the disease and improve patient outcomes. Additionally, targeting these early steps can provide broad-spectrum antiviral activity, as many viruses share similar entry mechanisms.

Spike (S) protein plays a key role in the attachment and entry of CoVs to host cells. The S protein is a class I fusion transmembrane structural glycoprotein which consists of S1 and S2 subunits. The S1 subunit consists of N-terminal domain (NTD) and receptor binding domain (RBD) and plays a crucial role in the process of binding to the cellular receptor. The S2 subunit, comprised of fusion peptide (FP), heptad repeat 1 (HR1), heptad repeat 2 (HR2), transmembrane domain (TM), and cytoplasmic domain fusion (CP), is responsible for mediating viral fusion and entry[10]. Initially, the RBD of S1 binds to the SARS-CoV-2 receptor angiotensin-converting enzyme 2 (ACE2) and is activated by cellular proteases to permit insertion of FP subunit into the host membrane[11]. Subsequently, the HR1 and HR2 regions form a six-helix bundle (6-HB), which pulls the viral and cellular membranes together and mediates fusion, resulting in the release of the viral genome into the cytoplasm to produce new viral particles[3]. Disruption of the interaction between HR1 and HR2 can lead to incomplete fusion, thereby inhibiting virus proliferation[12]. Therefore, the blockade of HR1/HR2 interaction should be an effective anti-SARS-CoV-2 strategy. Currently, some HR sequence-based lipopeptides such as HR2 sequence-based EK1 lipopeptides and IPB01 lipopeptides[13-15], HR1 sequence-based inhibitors HR1LS and HR121[16,17], HRC-derived lipopeptide[18], and some drugs such as Itraconazole and Estradiol benzoate[19], are reported to have inhibitory effects on SARS-CoV-2 infection by blocking HR1/HR2 interaction. Besides, short amino-acid sequences are highly conserved in the HR region among the CoVs but are dissimilar to any of the sequences in the human body[20]. So, HR1/HR2 interaction inhibitors may have broad spectrum anti-CoVs activity while being relatively safe.

Nowadays, FP-based assay, *in silico* design and pseudoviral system are the main methods employed for SARS-CoV-2 fusion inhibitor discovery[20-23]. For FP-based assay, the large deviation of fluorescence signals caused by trace screening volume and the fluorescence of compounds themselves can reduce the stability of screening which leads to false positives or false negatives. Special fluorescent substrates may also result in higher screening costs. Meanwhile, *in vitro* screening often lead to inactive agents during *in vivo* tests. For virtual screening based on *in silico* design, the discovery of effective inhibitors depends on the precise selection of screening pockets. However, the current HR1 and HR2 interaction inhibitors lack a precise screening pocket for virtual docking[24], significantly limiting their use in virtual screening. Additionally, false positives are common due to their low cellular penetration for compounds from *in silico* screening. As a cellular evaluation model, the pseudoviral system can more accurately assess whether the lead compounds screened from *in vitro* activity exhibit antiviral activity. However, it requires specialized laboratory facilities, and the high cost of luminescence detection significantly restricts its use in high-throughput screening (HTS) applications. Therefore, the establishment of a low-cost, low-false positive rate, direct, and easy-to-use screening method for HR1/HR2 interaction inhibitors is still necessary.

In this study, we developed an HTS model for HR1/HR2 interaction inhibitors using Yeast Two Hybrid (H2Y) system. Among 15,000 compounds, a small molecule inhibitor named IMB-9C was identified which showed anti-SARS-CoV-2 activity. Furthermore, the binding mode of IMB-9C with HR peptides and key amino acid sites has been identified. Based on these findings, IMB-9C can be regarded as a new structural backbone for further antiviral development.

2. Materials and methods

2.1. Cell culture

Huh-7 (human hepatocellular carcinoma), Vero (African Green Monkey Kidney), BHK-21 (Baby Hamster Syrian Kidney), HEK-293T (Human Embryonic Kidney 293T) and HEK-293T/ACE2 (HEK-293T overexpressing ACE2) cells were kept in DMEM (Hyclone, Mountain View, CA, USA) supplemented with 10% heat-inactivated fetal bovine serum (FBS, Gibco, Grand Island, NY, USA) at 37 °C in a humidified 5% CO_2 incubator. Vero E6/TMPRSS2 (Vero E6 overexpressing TMPRSS2) cells were maintained in DMEM culture medium supplemented with 10% heat-inactivated FBS and 2% Geneticin. Calu-3 (Human lung adenocarcinoma (thoracic water)) cells were cultured in MEM

Please cite this article as: Zhang Jing et al., Yeast-two-hybrid based high-throughput screening to discover SARS-CoV-2 fusion inhibitors by targeting the HR1/HR2 interaction, Acta Pharmaceutica Sinica B, https://doi.org/10.1016/j.apsb.2025.06.029

(Hyclone, Mountain View, CA, USA) supplemented with 10% heat-inactivated FBS and NEAA.

2.2. Viruses

The SARS-CoV-2 HKU-001 (a strain-wild type strain, WT) (GenBank accession number: MT230904) was isolated from the nasopharyngeal aspirate specimen of a patient who was laboratory-confirmed to have COVID-19 in Hong Kong. All the other variants, including Beta, Delta, Ba.1, Ba.2, Ba.4 and Ba.5 were previously isolated in Hong Kong. All experiments involving live SARS-CoV-2 followed the approved standard operating procedures of the biosafety level 3 facility at the University of Hong Kong and Sanford Burnham Prebys Medical Discovery Institute, as previously described[25].

2.3. Y2H assay

The Y2H system (Clontech, USA) includes AH109 strain, pGBKT (activation domain, AD), pGADT7 (DNA binding domain, BD), and control plasmids of pAD-T, pBD-53, and pBD-lam. The construction of Y2H system was based on a previously reported method[26]. In brief, the synthesized DNA fragments that encode full-length HR1 (aa918-983) and HR2 (aa1162-1203) (GenScript, Nanjing, China) were inserted into pGBKT and pGADT7 to generate plasmids pAD-HR1 and pBD-HR2. These two plasmids were then co-transferred into AH109 yeast strain by LiAc to get AH109 (pAD-HR1+pBD-HR2). Similarly, AH109 (pBD-HR2+pAD) and AH109 (pAD-HR1+pBD) were obtained to exclude self-activation. Strains AH109 (pAD-T + pBD-53) and AH109 (pAD-T + pBD-lam) were used as positive or negative control. All these strains were incubated on synthetic double dropout (SD) plates lacking leucine and tryptophan (SD/-Leu/-Trp) (Clontech, Mountain View, CA, USA) and incubated at 30 °C for 2−3 days. The positive transformants were further streaked onto SD/-Leu/-Trp/-Ade/-His plates and incubated at 30 °C for 3−4 days to examine the growth. Expression of HR1 and HR2 in positive clones was verified by Western blot using anti-myc and anti-HA monoclonal antibodies (Clontech, Mountain View, CA, USA).

2.4. β-Galactosidase (β-gal) activity assay

HR1/HR2 interaction of positive clones was further detected by β-gal activity assay as described previously[27]. In brief, after incubation in SD/-Leu/-Trp medium at 30 °C for 48 h, yeast cells were quickly frozen in liquid nitrogen and thawed at 30 °C over and over again until completely lysed. Then yeast solution was transferred onto filter paper and Z buffer/X-gal solution (0.1 mol/L Na_2HPO_4, 35 mmol/L NaH_2PO_4, 10 mmol/L KCl, and 1 mmol/L $MgSO_4$, pH 7.0, 0.4 mg/mL X-gal and 0.27% β-mercaptoethanol) was added to the paper, after which the color change was observed.

As β-gal can hydrolyze the colorless substrate *o*-nitrophenyl β-D-galactosidide (ONPG) to generate *o*-nitrophenol (ONP) which is bright yellow, β-gal activity quantitative detection kit (GENMED SCIENTIFICS INC. USA, Boston, MA, USA) was adopted to determine the relative level of β-gal activity in yeast cell extracts by measuring the absorbance at a wavelength of 420 nm. Enzyme activity could be calculated according to Eq. (1):

$$U = \frac{OD_{420\text{sample}} - OD_{420\text{blank}}}{OD_{600} \times t \times V} \quad (1)$$

where t is the incubation time (min) and V is the volume of cell cultures used for the assay (mL). The experiments were repeated three times.

2.5. HTS assay

The chemical compound library used for HTS assay in this research is a combination of synthetic compounds from Life Chemicals Inc. (Burlington, Canada). Compounds were stocked at 10 mg/mL in dimethyl sulfoxide (DMSO, Amresco, Framingham, MA, USA). The compounds in this library have undergone extensive selection, including prioritization of drug-likeness, novelty and rare chemotypes, virtual coupling of building block with in-stock reagents, saturation degree Fsp3 scoring (filtering by optimal physicochemical parameters: MW < 450, cLog$P$ <4.0, Lipinsky, Veber and in-house MedChem filters: reactivity, PAINS), expert estimation and pre-selection, as well as diversity. The screening assays were performed as described[28]. Briefly, for primary screening, freshly cultivated AH109 (pAD-HR1+pBD-HR2) cells (OD_{600} = 0.8) were diluted 100-fold in SD/-Leu/-Trp/-Ade/-His in 96-well plates (Corning, Corning, NY, USA). Then 199 μL of diluted culture and 1 μL of tested compounds (the final concentration was 50 μg/mL) or DMSO were added into each well. The growth inhibition of the yeast cells was assessed after 48 h incubation at 30 °C and the compounds that could completely inhibit the growth of AH109 (pAD-HR1+pBD-HR2) cells were selected as primary positive compounds. The minimum inhibitory concentration (MIC) of positive compounds against AH109 (pAD-HR1+pBD-HR2) were further detected, and AH109 (pAD-T + pBD-53) was used as negative control. The final concentration of the compounds ranges from 1.56 to 100 μg/mL with two-fold dilution. MIC endpoints were defined as the lowest concentration of drugs that completely inhibit the growth of yeast. Compounds with MIC against AH109 (pAD-HR1+pBD-HR2) lower than that of AH109 (pAD-T + pBD-53) by two times were selected for further research.

2.6. Pseudotyping of VSV and pseudotype-based inhibition assay

VSV pseudotyped with S protein from different variants of SARS-CoV-2 (wildtype, Alpha, Beta, Delta, Gamma, Mu, Ba.2) were generated as previously reported with some modifications[29]. In brief, BHK-21 cells (Kerafast, Boston, MA, USA) overexpressing S protein were inoculated with VSV-G pseudotyped ΔG-luciferase VSV (Kerafast, Boston, MA, USA). After a 2 h inoculation at 37 °C, the inoculum was removed and cells were incubated with DMEM supplemented with 5% FBS and VSV-G antibody (I1, mouse hybridoma supernatant from CRL-2700; ATCC; 1:100). Pseudotyped particles were collected at 24 h after inoculation, then centrifuged at 1320 g to remove cell debris and stored at −80 °C until use.

To determine the effect of the compound on viral entry, different concentrations of IMB-9C (from 0.8 to 100 μmol/L) diluted in DMSO were mixed with pseudovirus. HEK-293T/ACE2 cells were treated with IMB-9C and pseudovirus mixture for 24 h. The activity of firefly luciferase was measured using bright-Glo luciferase assay (E2620, Promega, Madison, WI, USA) for quantitative determination.

Please cite this article as: Zhang Jing et al., Yeast-two-hybrid based high-throughput screening to discover SARS-CoV-2 fusion inhibitors by targeting the HR1/HR2 interaction, Acta Pharmaceutica Sinica B, https://doi.org/10.1016/j.apsb.2025.06.029

2.7. Viral load reduction assay

A viral load reduction assay was performed on Vero E6/TMPRSS2 cells, as described previously with modifications[30]. A cytopathic assay was performed to detect antiviral effect for 72−96 h (MOI = 0.001). The concentration of a compound showing no cytopathic effect (CPE) was recorded as effective concentration (EC).

Supernatant samples from the infected cells were collected at 24 h.p.i. for qRT−PCR analysis of virus replication (MOI = 0.1). Briefly, 50 μL of viral supernatant was lysed with 70 μL of RLT buffer and then extracted for total RNA with the QIAamp viral RNA mini kit (Qiagen, Dusseldorf, German). Real-time one-step qRT-PCR was used for quantitation of SARS-CoV-2 viral load using the one-step Probe RT-PCR kit (Takara Bio (Beijing) Inc., Beijing, China) with a LightCycler 480 Real-Time PCR System (Roche, Basel, Switzerland) as previously described[25]. Each 20 μL reaction mixture contained 10 μL of 2 × one-step Probe RT-PCR Master Mix, 7 μL of RNase-free water, 1.6 μL each of 10 μmol/L forward and reverse primer, 0.4 μL of 10 μmol/L probe and 1 μL of extracted RNA as the template. Reactions were incubated at 45 °C for 10 min for reverse transcription, 95 °C for 5 min for denaturation, followed by 45 cycles of 95 °C for 5 s and 55 °C for 30 s. Signal detection was carried out and measurements were made in each cycle after the annealing step. The cycling profile ended with a cooling step at 40 °C for 30 s. The primers and probe sequences were against the RNA-dependent RNA polymerase/helicase (RdRP/Hel) gene region of SARS-Cov-2, as we previously described[25].

RdRp_SARSr-F2: CGCATACAGTCTTRCAGGCT.

RdRp_SARSr-R1: GTGTGATGTTGAWATGACATGGTC.

RdRp_SARSr-P2: FAM-TTAAGATGTGGTGCTTGCATACG TAGAC-lABkFQ.

2.8. Cell cytotoxicity assay

The cytotoxicity of compounds was examined on Huh-7, Vero and HEK-293T. After the cells (5000/well) were seeded in 96-well plates and grown to log-phase, compounds at various concentrations in DMEM medium without FBS were added in triplicate. 48 h later, 10 μL of the Cell Counting Kit-8 (CCK-8, Biosharp, Hefei, China) solution was added to each well, and the mixtures were incubated for another 4 h. The absorbance of each well was measured at 450 nm using a Microplate reader (PerkinElmer, Waltham, MA, USA). The IC_{50} values were calculated according to the concentration−response curve.

2.9. Native polyacrylamide gel electrophoresis (N-PAGE)

N-PAGE was used to detect the effect of IMB-9C on the interaction of HR1/HR2[31]. HR1P and HR2P (GL Biochem (Shanghai) Ltd., Shanghai, China) were mixed with final concentration of 40 μmol/L and then serially diluted IMB-9C was added with final concentration from 1.56 to 25 μmol/L. The sample treated with DMSO was used as control. After incubating at 37 °C for 1 h, all the samples were treated with non-denaturing buffer (Shanghai Wanshenghaotian Biotechnology inc., Shanghai, China). Then the samples were loaded on a Tris-glycine gel (18%) for 3 h and stained with Coomassie blue (Beyotime, Shanghai, China). The polypeptides were imaged using a ChemiDoc MP Imaging System (Bio-Rad, Hercules, CA, USA).

2.10. Cell−cell fusion assay

The establishment and detection of SARS-CoV-2 S-mediated cell−cell fusion assay was modified from a previously described protocol[32]. In short, HEK-293T cells transfected with a recombinant plasmid pAAV-IRES-EGFP-SARS-CoV-2-S (Genscript, Nanjing, China) encoding both EGFP and SARS-CoV-2 S glycoprotein (HEK-293T/EGFP/SARS-CoV-2-S) were used as effector cells with Vero E6/TMPRSS2 (adopting both plasma membrane fusion and endosomal fusion), HEK-293T/ACE2 (adopting endosomal fusion) and Calu-3 (adopting plasma membrane fusion) cells as the target cells, respectively. HEK-293T cells transfected with the original plasmid of pAAV-IRES-EGFP (Youbio, Chongqing, China) expressing only EGFP were set as negative control cells. Vero E6/TMPRSS2 were pre-treated with Camostat (50 μmol/L) or E64d (50 μmol/L) at 37 °C for 2 h[33]. Then Vero E6/TMPRSS2, HEK-293T/ACE2 and Calu-3 cells were co-cultured with effector cells at a rate of 1:1 in the absence or presence of IMB-9C at the final concentrations as indicated (12.5, 25, and 50 μmol/L), respectively. After co-cultivation at 37 °C for 12 h, syncytium formation between HEK-293T/EGFP/SARS-CoV-2-S and target cells were observed under high content analysis systems (PerkinElmer, Waltham, MA, USA).

2.11. Surface plasmon resonance (SPR) assay

The binding possibility between IMB-9C and HR1P or HR2P was determined by SPR spectroscopy (Reichert 2SPR, Buffalo, NY, USA) with the running buffer (1 × PBS Tween™−20 plus 5% DMSO). After activated and quenched with ethanolamine buffer (1 mol/L, pH 8.0), the surface of CM5 gold biosensor (Reichert Inc., Depew, NY, USA) was immobilized by either HR1P or HR2P. IMB-9C at given concentrations ranging from 1.56 to 25 μmol/L was flowed over the peptide-coated sensor with a contact time of 90 s. The dissociation kinetic was recorded within 330 s. The real RIU was continuously monitored, and the relationship between RIU and an arbitrary resonance unit (RU) was defined as 1 μRIU = 0.733 RU. Both association (K_{on}) and dissociation (K_{off}) constant values were determined by TraceDrawer 1.7.1 (Ridgeview Instruments, Uppsala, Sweden). The dissociation constant (K_D) was calculated by Eq. (2):

$$K_D = \frac{K_{off}}{K_{on}} \tag{2}$$

2.12. Intact protein analysis

To clarify the binding mode of HR1/HR2 with IMB-9C, protein molecular weight was confirmed by High Performance Liquid Chromatography-Quadrupole-Time-of-Flight Mass Spectrometry (HPLC−Q-TOF−MS) (Agilent, Palo Alto, CA, USA). Purified SARS-CoV-2 HR1 or HR2 (5 μmol/L) was incubated in the presence or absence of IMB-9C (500 μmol/L) in TBS (10 mmol/L Tris and 50 mmol/L NaCl, pH 8.0) at RT for 30 min, respectively. The molecule weight of the free SARS-CoV-2 HR1 or HR2 and IMB-9C treated with SARS-CoV-2 HR1 or HR2 were determined. Mass spectrum was deconvoluted using MassHunter software (Agilent, Palo Alto, CA, USA), and maximum entropy was performed for deconvolute algorithm. Mass spectrum data were saved and processed using FlexControl 3.4 (FLEXCONTROL, Noerre Nebel, Denmark).

Please cite this article as: Zhang Jing et al., Yeast-two-hybrid based high-throughput screening to discover SARS-CoV-2 fusion inhibitors by targeting the HR1/HR2 interaction, Acta Pharmaceutica Sinica B, https://doi.org/10.1016/j.apsb.2025.06.029

2.13. Circular dichroism (CD) spectroscopy assay

HR1P and HR2P were mixed with final concentration 10 μmol/L in PBS (50 mmol/L sodium phosphate, 150 mmol/L NaCl, pH 7.2) and then treated with IMB-9C (10 μmol/L) or 8.89 ‰ DMSO for 30 min at RT. CD spectral scanning in the far ultraviolet region (190−260 nm) was performed with CD spectrometer (Applied Photophysics, Leatherhead, UK). Each sample was scanned three times with a time constant of 1 s and a bandwidth of 1 nm. CDNN software (CEVA Inc., DE, USA) was employed to fit and deconvolute CD data to determine the relative number of α-helix, β-turn, β-sheet, and randoms.

2.14. Molecular docking

To identify the possible binding mode of IMB-9C with HR1, the crystal structure of post fusion core of SARS-CoV-2 S2 subunit (PDB ID: 6LXT; https://www.rcsb.org/structure/6lxt) was obtained from Protein Data Bank (PDB). In our docking research, the pocket of HR1 was the whole protein of HR1. At the beginning of the docking study, water molecules were separated from the PDB files and polar hydrogens were added simultaneously to the same PDB file. On the other hand, PDB structures of ligand molecules were created using ACD chemsketch software (https://www.acdlabs.com/resources/freeware/chemsketch/), which were subsequently changed into pdbqt format with the help of AutoDock Vina software.

A docking program Autodock vina[34] was applied to calculate the interaction between nine flexible structures of IMB-9C with the rigid binding sites. After docking, the conformation of the compound was analyzed, and the (H bond and hydrophobic) interactions and three-dimensional models were generated with UCSF Chimera[35], LIGPLOT[36], or PyMol (Schrodinger LLC, New York, NY, USA).

2.15. Site-directed mutagenesis

$HR1_{mutant}$ genes with substitutions of Glycine codon at A930, I931, K933, I934, Q935, S937, L938, S939, S940, T941, T942, L945 sites were synthesized by GenScript (Nanjing, China). AH109 (pAD-$HR1_{mutant}$ + pBD-HR2) was constructed according to that of the AH109 (pAD-HR1+pBD-HR2).

2.16. ADMET analysis

The free web tool SwissADME (www.swissadme.ch/) was utilized to predict the pharmacokinetic (PK), drug-likeness, and medicinal chemistry friendliness of IMB-9C[37]. The 2D structure of IMB-9C was drawn *via* ChemDraw Ultra version 10 and subsequently converted into the SMILES format. Then druglikeness prediction was conducted through SwissADME to generate the data[38] for in-depth analysis[39].

2.17. In vitro metabolic stability within human liver microsomes (HLMs)

A LC−MS/MS analytical method was used to analyze the metabolism of IMB-9C in HLMs *in vitro*. Briefly, 155 μL of sample solution (including 1 μL of 200 μmol/L IMB-9C or Verapamil plus 154 μL of 0.1 mol/L PBS) and 5 μL of HLMs (IPHASE, China) were incubated at 37 °C for 5 min. Then NADPH generating solution, which was freshly prepared by mixing solution A ($NADP^+$; Glc-6-PO_4; $MgCl_2$), solution B (G6PDH), and PBS (pH 7.4, 0.1 mol/L) at the ratio of 5:1:14, were added to initiate the reaction at 37 °C. The group without NADPH was served as the negative control to exclude the metabolism of the compound itself in the reaction system, and the group without compound was used as the blank control. At given time points (0, 15, 30, 45, 60, and 120 min for IMB-9C, and 0, 10, 15 and 30 min for positive control verapamil), aliquots were withdrawn on ice and the reaction was quenched by 200 μL of pre-cooled acetonitrile. The content of the sample at 0 point was set to 100%. The samples were then subjected to vortex mixing for 3 min, followed by centrifugation at 15,180×*g* for 3 min. The resulting supernatant was further determined for its concentration. All the data analyses were performed using GraphPad Prism (GraphPad Software, San Diego, CA) and the data were mean ± standard deviation (SD).

2.18. Plasma stability analysis

10 μL of IMB-9C (200 μmol/L) or Propantheline Bromide (the positive control, 200 μmol/L) were introduced into 390 μL of plasma solutions (IPHASE Plasma, Single Donor, Male, Customize, Heparin Sodium). Then 50 μL of the mixture was immediately removed and 300 μL of pre-cooled acetonitrile was added. The remaining mixture was incubated at 37 °C and every 50 μL were taken out at different time points (15, 30, 45, 60, and 120 min for IMB-9C, 15, 30, and 10, 20, 30 and 40 min for propantheline bromide). After that 300 μL of pre-cooled acetonitrile was added to terminate the reaction (for propantheline bromide: 30 μL of mixture was taken out and 1000 μL of pre-cooled acetonitrile was added for termination). At last, the mixture left was vortexed for 30 s, placed on ice, shaken at 3803×*g* for 3 min and centrifuged at 17,605×*g* for 3 min successively. The obtained supernatant was subjected to LC−MS/MS analysis. The content of the sample at 0 point was set to 100%.

2.19. Statistical analysis

GraphPad Prism 9.0 was used for statistical analyses and figure plotting. The statistical significance of differences was determined by Student's *t*-test for comparison between One-way analysis of variance. All quantitative data were from three independent experiments. $P < 0.05$ was considered to indicate a statistically significant difference.

3. Results

3.1. HTS targeting SARS-CoV-2 HR1/HR2 interaction

3.1.1. Confirmation of SARS-CoV-2 HR1/HR2 interaction by Y2H system

HR1 and HR2 are known to interact with each other, which is crucial for the translocation of SARS-CoV-2 into host cells[6] (Fig. 1). To identify inhibitors targeting HR1/HR2 interaction, a Y2H system was constructed to confirm this interaction. In this system, the HR1 and HR2 encoding genes from SARS-CoV-2 were fused in frame to the activating domain of Gal4 transcription factor and Gal4 DNA binding domain. The interaction between HR1 and HR2 can restore the function of Gal4 promoter leading to the activation of three reporter genes ADE2, HIS3, and LacZ, which can be confirmed by the growth of Y2H system on plates SD/-Ade/-His and LacZ-dependent color change.

Please cite this article as: Zhang Jing et al., Yeast-two-hybrid based high-throughput screening to discover SARS-CoV-2 fusion inhibitors by targeting the HR1/HR2 interaction, Acta Pharmaceutica Sinica B, https://doi.org/10.1016/j.apsb.2025.06.029

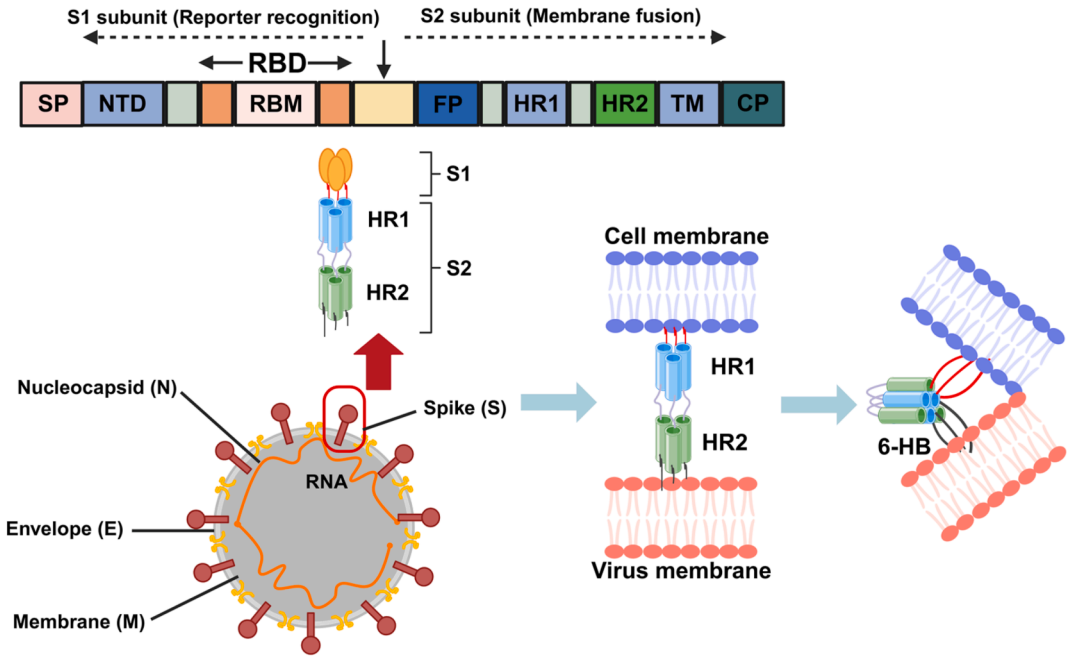

Figure 1 Graphic diagram for HR1/HR2 mediated translocation of SARS-CoV-2 into host cells. SARS-CoV-2 uses surface spike protein (S protein) to enter host cells. The S protein is composed of two subunits: S1 and S2. S1 is responsible for receptor recognition. After binding with host cell receptor, S1 is cleaved by host cell proteases to expose highly hydrophobic membrane-binding domains of the S2 subunit, namely heptad repeat domain 1 (HR1) and heptad repeat domain 2 (HR2). Then HR1 and HR2 form a thermodynamically favorable six-helix bundle (6-HB) post-fusion structure to fuse the viral and cellular membranes together.

Compounds blocking the interaction between HR1 and HR2 can inhibit the growth of this Y2H system and reduce the production of β-gal (Fig. 2A).

As shown in Fig. 2B and C, positive control AH109 (pAD-T + pBD-53) also grew well on a SD/-Ade/-His dropout plate and could display strong β-gal activity because of the interaction between the expressed proteins p53 and SV40-T. In contrast, AH109 (pAD-T + pBD-lam) (human lamin C), the negative control, could not grow on the dropout plate. AH109 (pAD-HR1+pBD-HR2) grew well on a SD/-Ade/-His dropout plate and could display strong β-gal activity which validated the existence of interaction between HR1 and HR2. But we did not obtain AH109 (pAD-HR2+pBD-HR1), which indicated that this fusion expression pattern might affect the interaction between HR1 and HR2. Yeast cells harboring either pAD-HR1 or pBD-HR2 alone did not show growth and were negative for β-gal activity, eliminating the possibility of self-activation. The expression of HR1 and HR2 in yeast cells was also validated by Western blot (Fig. 2D). Therefore, the SARS-CoV-2 HR1/HR2 interaction was confirmed by Y2H system which can be further used for inhibitor screening.

3.1.2. *HTS for compounds that block HR1/HR2 interaction*

Known HR1/HR2 interaction inhibitor Itraconazole[19] was utilized to validate whether the Y2H model could be applied to HTS. As shown in Fig. 3A, the MIC of Itraconazole towards AH109 (pAD-HR1+pBD-HR2) was 3.125 μg/mL with the MIC towards AH109 (pAD-T + pBD-53) being 12.5 μg/mL, indicating specific blockage towards HR1/HR2 and proving the feasibility of this Y2H system in subsequent HTS.

In the initial screening, the growth inhibitory activity of compounds at 50 μg/mL against AH109 (pAD-HR1+pBD-HR2) in SD/-Leu/-Trp/-Ade/-His medium was detected, and 50 compounds completely inhibited the growth of AH109 (pAD-HR1+pBD-HR2) were selected from 15,000 compounds. In order to further exclude the inhibitory activity of compounds against AH109 itself or Gal4 expression system, the MIC of initially 50 compounds on AH109 (pAD-HR1+pBD-HR2) was detected, with AH109 (pAD-T + pBD-53) as the negative control. 32 compounds with MIC for AH109 (pAD-HR1+pBD-HR2) lower than those for AH109 (pAD-T + pBD-53) by more than 2 times were selected as positive for the second screening. To further confirm their selective blockage on HR1/HR2 interaction, AH109 (pAD-HR1+pBD-HR2) were subjected to a quantitative β-gal assay in the presence of different concentrations of the hit compounds. Among the 32 hits, the inhibition rates of IMB-2B, 5C, 9C, and 11B were higher than 50% at the concentration of their 1/2 MIC, respectively, and were all in concentration dependent manners (Fig. 3B and Supporting Information Fig. S1). MIC values of the four compounds against Y2H were shown in Table 1.

3.1.3. *Inhibition against pseudotyped SARS-CoV-2 infection*

The selected four hits from HTS were applied for wildtype (WT) pseudovirus assay to evaluate their anti-entry potential at 45 μmol/L and IMB-9C emerged as the most promising candidate as the only one exhibited anti-viral activity above 50%, with an inhibition rate of 75.88%. Further test for the inhibitory activity of IMB-9C on pseudovirus showed that it exhibited a dose-dependent inhibitory effect on viral entry with EC_{50} of 32.15 μmol/L (Fig. 3C). Then various pseudoviruses were utilized to evaluate its efficacy. Notably, IMB-9C demonstrated enhanced potency against Omicron variants compared with WT and previous variants with EC_{50} values summarized in Table 2. So, in the end, IMB-9C was chosen for in-depth research. The whole screening process is shown in Fig. 3D.

Please cite this article as: Zhang Jing et al., Yeast-two-hybrid based high-throughput screening to discover SARS-CoV-2 fusion inhibitors by targeting the HR1/HR2 interaction, Acta Pharmaceutica Sinica B, https://doi.org/10.1016/j.apsb.2025.06.029

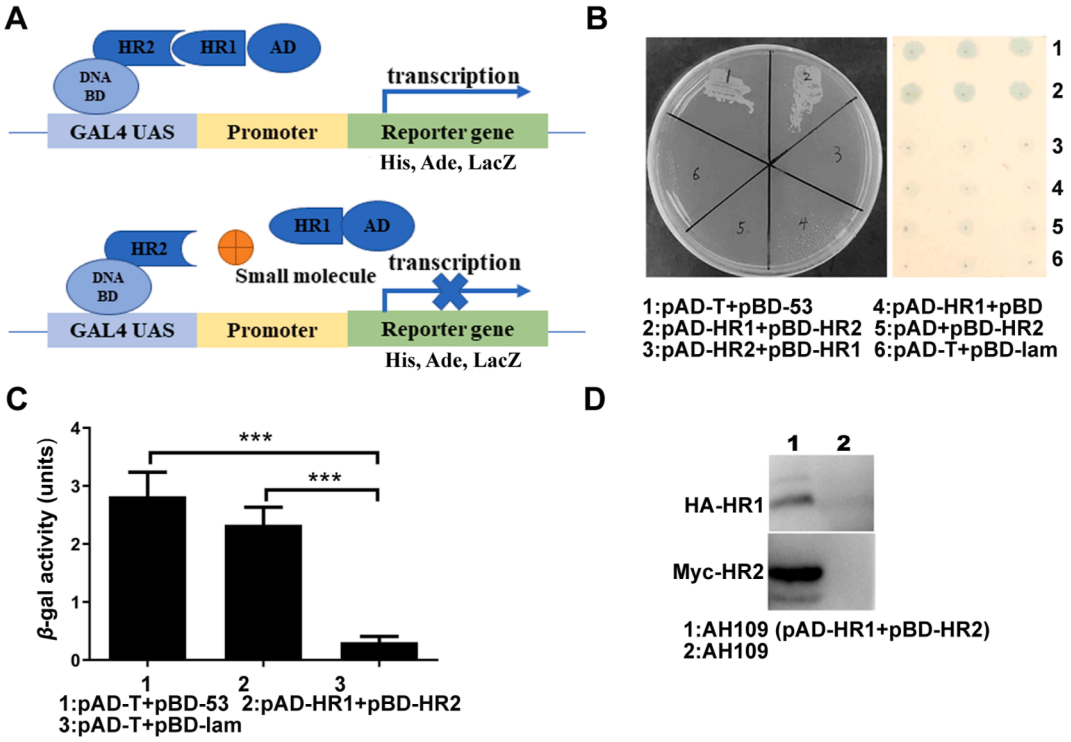

Figure 2 Validation of SARS-CoV-2 HR1/HR2 interaction in Y2H system. (A) Principle of Y2H system and screening strategy for HR1/HR2 interaction inhibitors. The interaction between HR1 connected to the transcriptional activation domain (AD) and HR2 connected to the DNA binding domain (BD) allowed BD and AD to be sufficiently close in space, restoring the function of the transcription factor Gal4, subsequently led to the expression of the reporter genes ADE2, HIS3, and LacZ which can be disrupted by the inhibitor of HR1/HR2 interaction. (B) The growth of AH109 cells with various combinations of BD and AD fusion on an SD/-Leu/-Trp/-Ade/-His dropout plate (left panel) and their LacZ-dependent color change (right lane). Filter paper bearing lysed colonies from selective plates was overlaid with X-gal buffer. Noticeable color change could be observed following an overnight incubation for AH109 (pAD-T + pBD-53) and AH109 (pAD-HR1+pBD-HR2). (C) Quantification of β-gal activity in Y2H system. Lysis buffer, enhancement buffer, active buffer, and lysis buffer were successively added to the fresh yeast precipitation to make sure that the yeast cells were fully broken. Add diluent solution and reaction solution separately to the yeast supernatant and start timing until a bright yellow color appears. Add termination solution and record the reaction time. Absorbance at wavelengths of 420 and 600 nm was measured immediately. The data were shown as mean ± SD from triplicate assays. ***$P < 0.001$ (D) The expression of HR1 and HR2 in newly built Y2H system detected using anti-HA and anti-Myc antibodies.

3.2. *Antiviral activity and cytotoxicity of IMB-9C*

The antiviral activity of IMB-9C was further tested on live virus with CPE assay and q-PCR. The results revealed IMB-9C was efficient in inhibiting virus-induced CPE for WT, Beta, Delta, Ba.1, Ba.2, Ba.4 and Ba.5, with IC_{50} s at μM level ranged from 0.4 to 3.1 μmol/L and SI values all above 70 as Table 3. Meanwhile, q-PCR was performed to verify the CPE assay results. The EC_{50} of IMB-9C against WT strain was 1.952 μmol/L. More importantly, IMB-9C exhibited low toxicity on mammalian cells such as HEK-293T, Huh-7 and Vero cells.

3.3. *IMB-9C could block the interaction between HR1/HR2 by binding with both HR1 and HR2*

3.3.1. *IMB-9C blocked interaction between HR1 and HR2 of SARS-CoV-2*

N-PAGE is a polyacrylamide gel electrophoresis method for proteins that remain active without addition of denatured agents, which has been successfully applied to test the formation of 6-HB structures of type I fusion proteins[40,41]. In this study, N-PAGE was adopted to detect the disruption of 6-HB formation between SARS-CoV-2 HR1 and HR2 by IMB-9C. As shown in Fig. 4A, the individual HR1P containment negative charges that drove the peptide upward and off the gel under the negatively charged electrophoresis condition, with no bands shown in the gel (lane 2), while the free HR2P with net negative charge migrated downwards and showed a band in the lower part of the gel (lane 3). The HR1P/HR2P mixture showed a band on the upper part of the gel at about 26 kDa (lane 4) which represented 6-HB formation between HR1P and HR2P. But for HR1P/HR2P mixture treated with IMB-9C, the density of the band (lane 5−9) decreased. These data suggested that IMB-9C was able to block 6-HB formation between HR1 and HR2.

3.3.2. *IMB-9C inhibited SARS-CoV-2-S-mediated cell−cell fusion*

SARS-CoV-2 utilizes two distinct pathways for cell entry: transmembrane serine protease 2 (TMPRSS2)-mediated pathway, also called plasma membrane fusion, and the cathepsin L (CTSL)-mediated pathway, also known as endosomal fusion[42]. In the former pathway, after recognition of S with ACE2, S is cleaved by TMPRSS2 at the cell surface leading to exposure of HRs to the environment, which in turn enables membrane fusion to occur. In

Please cite this article as: Zhang Jing et al., Yeast-two-hybrid based high-throughput screening to discover SARS-CoV-2 fusion inhibitors by targeting the HR1/HR2 interaction, Acta Pharmaceutica Sinica B, https://doi.org/10.1016/j.apsb.2025.06.029

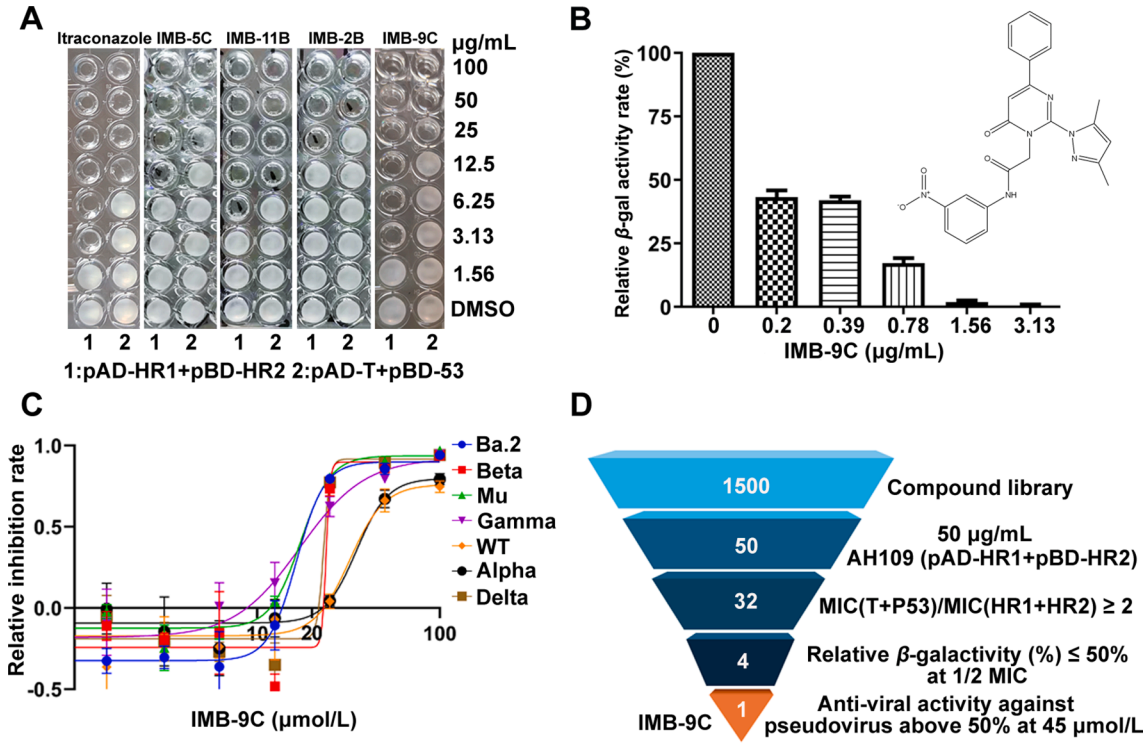

Figure 3 High throughput screening of inhibitors that disrupts HR1/HR2 interaction. (A) Growth inhibition of Y2H system by HR1/HR2 interaction inhibitors. AH109 cells with indicated plasmids were treated with hit compounds and Itraconazole (from 1.56 to 100 μg/mL) in 96-well plates in SD/-Leu/-Trp/-Ade/-His dropout medium for 48 h and the growth of cells was shown. (B) The inhibition of β-gal activity of IMB-9C against AH109 (pAD-HR1+pBD-HR2) cells and IMB-9C's structure. The data showed the ratio of β-gal activity of cells treated with compounds over that of untreated cells. The results were mean ± SD from triplicate assays. (C) The inhibitory activity of IMB-9C against pseudoviruses. The data showed the ratio of fluorescence of cells treated with IMB-9C over that of untreated cells. The results were from triplicate assays. (D) Summary of inhibitor screening. In the primary screen, 15,000 compounds were screened for HR1/HR2 interaction inhibitors and 50 compounds were selected which completely inhibited the growth of AH109 (pAD-HR1+pBD-HR2) at 50 μg/mL. Among them, 32 compounds showed stronger inhibitory activity for AH109 (pAD-HR1+pBD-HR2) than for AH109 (pAD-T + pBD-53) with MICs more than 2 times. From them, 4 compounds were selected with β-gal activity inhibitory rate higher than 50% at 1/2 MIC concentration. Finally, IMB-9C was selected as the most promising candidate that showed anti-pseudoviral activity above 50% at 45 μmol/L.

the CTSL-mediated pathway, SARS-CoV-2 initially undergoes internalization through endocytosis. Subsequently, the viral S is cleaved by CTSL within the endosomes, enabling the virus to release its genome into the host cells[43].

The cell−cell fusion system consists of two cell types, with target cells expressing host receptor and effector cells expressing viral fusion related factors. It is usually employed to evaluate the inhibitory activity of inhibitors on the process of entry into the host by virus. The role of the 6-HB structure formed by HR/HR2 during the fusion process between SARS-CoV-2 and cellular hosts can also be evaluated by this system[17,19,33].

In this study, we evaluated the inhibitory activity of IMB-9C against the two pathways in the presence of inhibitors that block one pathway (Camostat for TMPRSS2-mediated plasma membrane fusion [3] and E64d for endosomal fusion[44]). As entry of SARS-CoV-2 into Vero E6 cells is CTSL-dependent[45]. The stable expression of TMPRSS2 in Vero E6 cells endows Vero E6/TMPRSS2 cells with two pathways for SARS-CoV-2 entry. As shown in Fig. 4B−a large number of large cells (syncytium) were found in co-cultures of Vero E6/TMPRSS2 and HEK-293T/EGFP/SARS-CoV-2-S cells, representing cell fusion. Addition of Camostat or E64d had no significant effects on cell−cell fusion, but the number of fused cells decreased in a dose-dependent

Table 1 Inhibitory activity of hit compounds against Y2H system.

Strains	MIC(μg/mL)			
	IMB-9C	IMB-11B	IMB-2B	IMB-5C
AH109 (pAD-HR1+ pBD-HR2)	3.125	6.25	25	12.5
AH109 (pAD-T+ pBD-53)	12.5	12.5	50	50

Table 2 The IC_{50} (μmol/L) of IMB-9C against pseudoviruses.

Parameter	WT	Alpha	Beta	Mu	Gamma	Delta	Ba.2
IC_{50}	32.15	34.98	23.86	17.29	17.13	23.14	16.42

Please cite this article as: Zhang Jing et al., Yeast-two-hybrid based high-throughput screening to discover SARS-CoV-2 fusion inhibitors by targeting the HR1/HR2 interaction, Acta Pharmaceutica Sinica B, https://doi.org/10.1016/j.apsb.2025.06.029

Table 3 The IC_{50} (μmol/L) and CC_{50} (μmol/L) of IMB-9C against SARS-CoV-2 and its variants.

Parameter	WT	Beta	Delta	Ba.1	Ba.2	Ba.4	Ba.5
IC_{50}	3.1−1.6	1.6−0.8	1.6−0.8	0.8−0.4	0.8−0.4	0.4	0.8−0.4
CC_{50}	>112.5	>112.5	>112.5	>112.5	>112.5	>112.5	>112.5
SI*	>70.3	>140.6	>140.6	>281.3	>281.3	>281.3	>281.3

SI* = CC_{50}/IC_{50}.

manner within the samples treated with IMB-9C, indicating that IMB-9C could effectively inhibit SARS-CoV-2-S-mediated cell−cell fusion in both pathways.

Next, a single pathway cell fusion experiment was conducted to confirm the inhibition profile of IMB-9C. Since HEK-293T/ACE2 cells, endogenously expressing hACE2 and CTSL, preferentially utilize CTSL-dependent mechanism of SARS-CoV-2 entry[3], and Calu-3 cells, expressing high amounts of hACE2 and limited amounts of CTSL[46], employ a TMPRSS2-independent mechanism of SARS-CoV-2 entry. Both of them were employed as target cells to examine the sensitivity of cell−cell fusion to IMB-9C inhibition with HEK-293T cells expressing SARS-CoV-2 S as effector cells. Similar phenomenon was observed as cells treated with IMB-9C exhibited severe reduction in the number of generated multinucleated EGFP positive syncytia. These results further demonstrate that IMB-9C could inhibit both fusion pathways (Supporting Information Fig. S2). Overall, it seemed that IMB-9C relatively affected plasma membrane fusion over endosomal membrane fusion.

3.3.3. IMB-9C could bind to both HR1and HR2 in vitro

The binding profiles of compound IMB-9C with HR1 and HR2 were further determined by SPR. HR1 or HR2 was immobilized on a CM5 sensor chip, and then exposed to IMB-9C respectively at various concentrations. The SPR analysis showed that IMB-9C could bind to both HR1 and HR2, with K_D values as 5.67×10^{-7} and 3.68×10^{-5} mol/L, respectively (Fig. 4C, Table 4). IMB-9C showed stronger binding with HR1 than HR2 with about 100-fold difference, indicating it may mainly bind to HR1.

3.4. The binding mode of IMB-9C with HR1 and HR2

3.4.1. HPLC−Q-TOF−MS based study of SARS-CoV-2 HR1 or HR2 association with IMB-9C

Covalent conjugation can make the binding between two components tighter, and when using HPLC−Q-TOF−MS for molecular weight detection, it will be manifested as the sum of the molecular weights of the two components. To detect whether there is a covalent bond between IMB-9C and HRs, we incubated IMB-9C with HR1 or HR2 to observe the changes in molecular weight before and after incubation using HPLC−Q-TOF−MS. As shown as Fig. 4D, for HR1 and HR2 alone, the MS peak with a mass value of 4386.22 and 4007.27 Da were detected respectively. For HR1 or HR2 co-incubated with IMB-9C, there were no significant differences in the MS peak compared to the individual peptide samples, which were 4386.22 and 4007.34 Da, respectively, indicating non-covalent binding between IMB-9C and HR1 or HR2.

3.4.2. CD analysis of IMB-9C binding on the secondary structure of SARS-CoV-2 spike protein

The effect of IMB-9C on the structure of HR1+HR2 was further investigated by CD spectroscopy, which is a common tool to elucidate the secondary structure of polypeptides. HR1P and HR2P were co-incubated at RT for 30 min, then CD wave scanning was measured from 190 m to 260 nm at 4 °C. As shown in Fig. 4E and Table 5, the structure of HR1P + HR2P had a typical double negative peak at 208 and 222 nm. The percentage content of α-helix, β-fold and β-turn structure was 0.3%, 10.70% and 28.2% respectively. For HR1P + HR2P treated with IMB-9C, β-turn decreased by 11.70%, whereas the α-helix and β-fold contents increased by 19.80% and 28.07%, respectively, which indicated that IMB-9C influenced the secondary structure of the SARS-CoV-2 HR1P + HR2P.

3.4.3. The key binding sites of IMB-9C with HR1

Compared with HR2, HR1 showed stronger binding affinity with IMB-9C, so HR1 was selected for further study for its binding sites with IMB-9C. Computer-simulated docking utilizing a grid box that encompasses the full crystal structure of HR1 (PDB: 6lxt) indicated that IMB-9C might fit into the pocket between HR1 and HR2 alpha-helix structure (Fig. 5A). To clearly analyze the interaction between HR1 and IMB-9C by LigPlot+ in one conformation (Fig. 5A), direct hydrogen band with residue K933 and hydrophobic interactions with residues A930, I931, K933, I934, Q935, S937, L938, S939, S940, T941, T942, and L945 were indicated in two conformations. Other conformations were presented in Supporting Information Fig. S3.

We introduced structurally similar but non-reactive Glycine residue to replace these twelve amino acids respectively and constructed $HR1_{mutant}$/HR2 Y2H system to detect the interaction between $HR1_{mutant}$/HR2. We did not obtain Y2H systems with I934, Q935, S937, L938, S939, S940, and T942 site mutations, suggesting that these amino acids play important roles in HR1/HR2 interaction. Only the replacement of A930, I931, K933, T941, and L945 in parent Y2H could grow on the dropout plate. Compared with AH109 (pAD-HR1+pBD-HR2), the MICs of the IMB-9C against AH109 (pAD-$HR1_{mutant}$ + pBD-HR2) up-regulated 4−8 times, referencing a progressive loss of inhibitory activity of IMB-9C toward HR1/HR2 interaction (Table 6). To further verify the above evaluation, we additionally performed SPR to detect the affinity between IMB-9C and $HR1_{mutant}$. As presented in Fig. 5B and Table 7, the binding affinity of IMB-9C with A930, I931, K933, T941, and L945 mutated HR1P decreased by 2−3 orders of magnitude. All the results confirmed their critical roles in the binding of IMB-9C with HR1.

3.5. Druggability assessment of IMB-9C

3.5.1. Pharmacokinetic (PK) estimation for IMB-9C

Factors such as absorption, distribution, metabolism, elimination/excretion, and toxicity (ADMET) are considered as highly reliable screening filters for estimating PK properties of the candidate drugs (CDs)[47-49].

Please cite this article as: Zhang Jing et al., Yeast-two-hybrid based high-throughput screening to discover SARS-CoV-2 fusion inhibitors by targeting the HR1/HR2 interaction, Acta Pharmaceutica Sinica B, https://doi.org/10.1016/j.apsb.2025.06.029

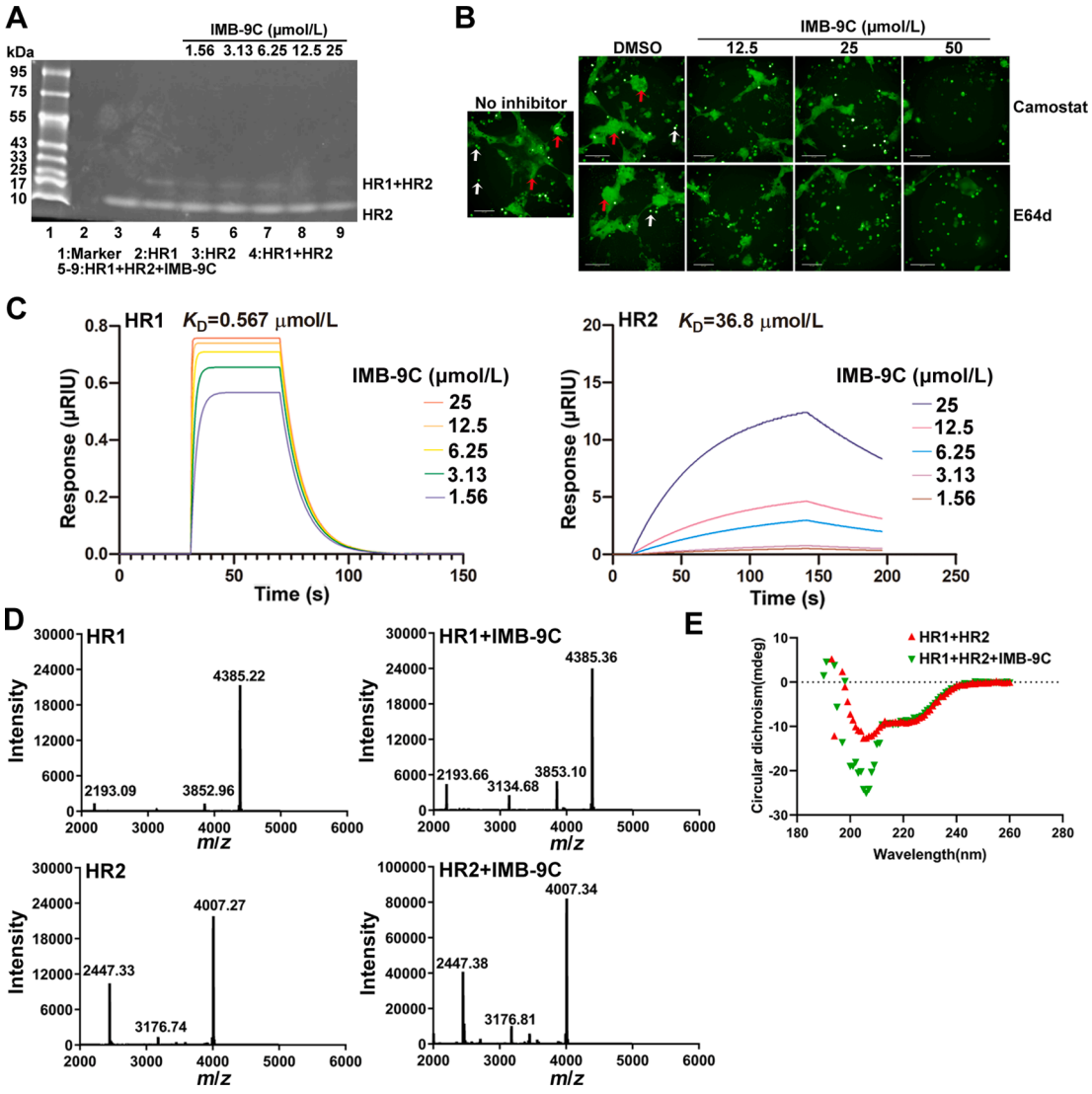

Figure 4 IMB-9C could block the interaction between HR1/HR2 by binding with both HR1 and HR2. (A) IMB-9C blocked the interaction of HR1/HR2 *in vitro*. The complex of HR1 and HR2 was treated with IMB-9C or DMSO (1%) and detected by N-PAGE under the negatively charged electrophoresis condition, while the free HR1P or HR2P was used as indicator. (B) IMB-9C inhibited SARS-CoV-2-S-mediated cell−cell fusion. Vero E6/TMPRSS2 (target cells) pretreated with either Camostat (50 μmol/L) or E64d (50 μmol/L) were co-cultured with HEK-293T/EGFP/SARS-CoV-2-S (effector cells) in the absence or presence of IMB-9C (12.5, 25, and 50 μmol/L). After co-cultivation at 37 °C for 12 h, syncytium formation was observed under high content analysis system. The white arrow indicated HEK-293T/EGFP/SARS-CoV-2-S and the red represented the fused cells. Scale bar is 200 μm. (C) SPR analysis for the binding of IMB-9C with HR1 and HR2. Serially concentrated solutions of IMB-9C (from 1.56 to 50 μmol/L) were injected into the chamber with a CM5 chip coated with HR1 or HR2. The change of response units was shown. (D) Compound IMB-9C interacted non-covalently with SARS-CoV-2 HR1P and HR2P. The molecular weights of SARS-CoV-2 HR1P or HR2P and IMB-9C in complex with SARS-CoV-2 HR1P or HR2P were determined using HPLC−Q-TOF−MS. The mass shift (Δm) of the protein is labeled. (E) Conformational influence of IMB-9C on HR1+HR2 complex. The secondary structure of HR1+HR2 with or without IMB-9C in PBS was examined by CD spectroscopy. Double minima at 208 and 222 nm were revealed.

SwissADME result presented in Table 8 revealed that IMB-9C adhered to Lipinski, Veber, Muegge, Egan, and Ghose rules with optimal PK values across generally acknowledged parameters, including molecular weight (444.44, which is between 150 and 500 g/mol), the sum of hydrogen-bond donors (1, meets the requirement of being <5), the sum of hydrogen-bond acceptors (6, satisfies the condition of being <10), the rotatable bonds (7, fulfills the criterion of being ≤10), Consensus Log PO/W (2.40, within the range of 2.25−4.75), and TPSA (127.63 Å^2, within the range of 20−130 Å^2). Meanwhile it cannot be ignored that water solubility (log S (Ali)[50] as −5.38) was not ideal enough. The thorough assessment also indicated a remarkable gastrointestinal (GI) absorption capacity for IMB-9C. IMB-9C was also confirmed

Table 4 The kinetics data of SPR analysis.

Sample	K_{on} (1/Ms)	K_{off} (1/S)	K_D (mol/L)
HR1	1.95×10^5	1.10×10^{-1}	5.67×10^{-7}
HR2	4.09×10^1	1.51×10^{-3}	3.68×10^{-5}

Please cite this article as: Zhang Jing et al., Yeast-two-hybrid based high-throughput screening to discover SARS-CoV-2 fusion inhibitors by targeting the HR1/HR2 interaction, Acta Pharmaceutica Sinica B, https://doi.org/10.1016/j.apsb.2025.06.029

Table 5 CD analysis/impact of IMB-9C on the secondary structure of HR1+HR2.

Sample	Secondary structure content (%)			
	α-elix	β-fold	β-turn	Random
HR1+HR2	0.3	10.70	28.20	61.20
HR1+HR2+IMB-9C	20.10	38.77	16.50	24.70

Table 6 MICs (μg/mL) of IMB-9C against HR1mutant/HR2 Y2H system.

Parameter	A930	I931	K933	T941	L945	Wild
MIC	50	25	25	12.5	12.5	3.125

to be a non-substrate for P-glycoprotein and unable to cross the blood−brain barrier. But investigation into drug metabolism unveiled its inhibitory potential against CYP2C19, CYP2C9, and CYP3A4 enzymes. Moreover, the bioavailability score of IMB-9C (0.55) was consistent and optimal.

3.5.2. *In vitro metabolic stability test in HLMs*

90% of drugs are metabolized by cytochrome P450s (CYP450s) in HLMs, so, the HLMs system provides a reliable basis to predict liver metabolism of drugs *in vivo*[51]. In this study, the stability of IMB-9C was further researched using HLMs system. In the -NADPH-free group, the content of IMB-9C (120 min) and the positive control verapamil (30 min) exhibited no changes, with relative residual rate as 99.27% and 101.62% respectively, indicating that there was no deviation of enzyme metabolism result caused by the chemical instability of compounds. In the group with-NADPH, the verapamil was almost completely degraded within 30 min, while IMB-9C showed a lower intrinsic clearance rate (25.2 ± 0.6 μL/min/mg) and a longer half-life period with $T_{1/2}$ = 55 ± 5.9 min (Supporting Information Fig. S4A).

3.5.3. *Plasma stability study of IMB-9C*

Plasma stability is crucial in determining the druggability of a lead compound[52]. As shown in Fig. S4B, the content of positive control propantheline bromide showed a time-dependent decrease in plasma,

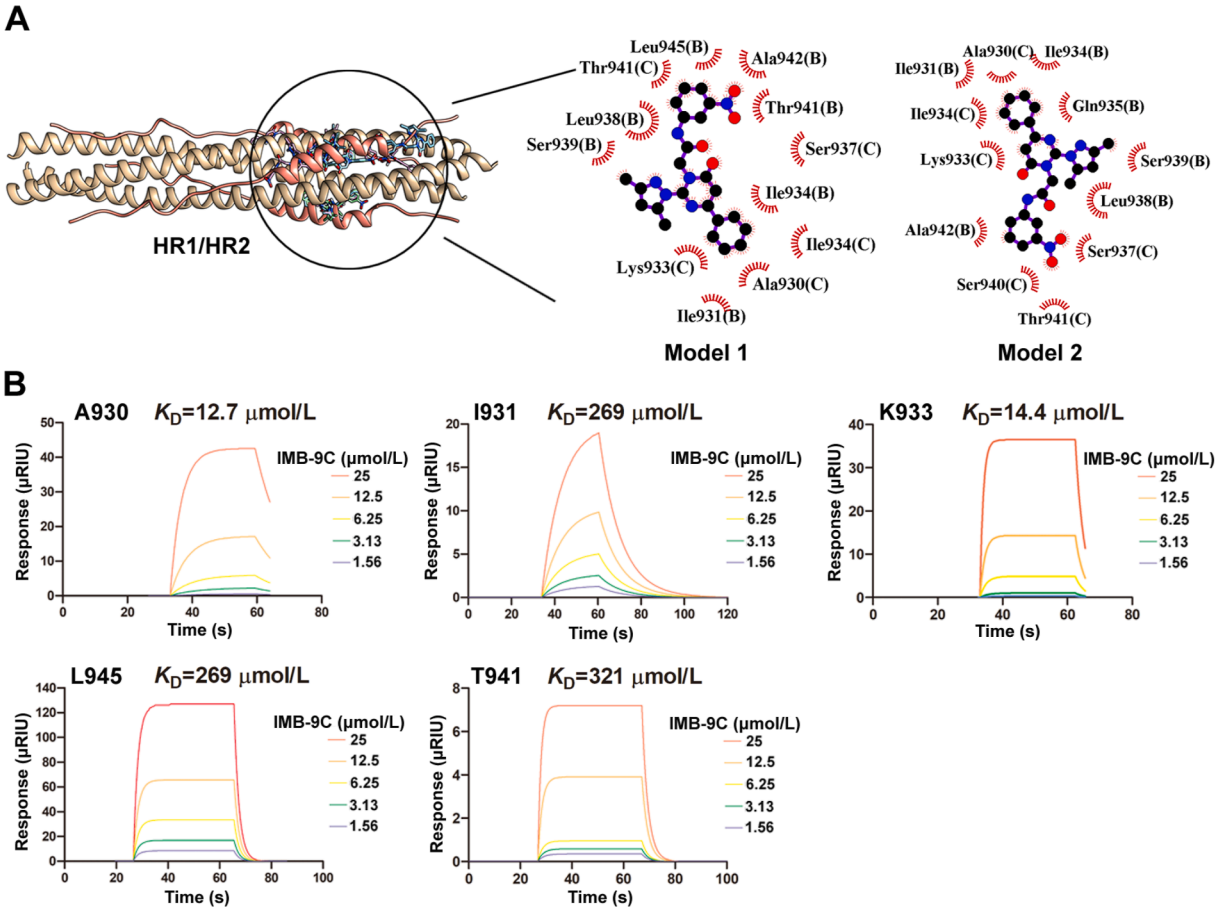

Figure 5 The binding mode of IMB-9C with HR1. (A) Details of interaction of IMB-9C in complex with SARS-CoV-2's HR1. HR1 and HR2 are shown as yellow and orange ribbon models, respectively. IMB-9C located at the interface where HR1 and HR2 interacted. Hydrophobic contacts are represented by an arc with spokes radiating towards the IMB-9C atoms that they contact. The contacted atoms in IMB-9C are shown with spokes radiating back. (B) SPR analysis of the physical interaction between IMB-9C with HR1 mutations at A930, I931, K933, T941, L945. After immobilizing the $HR1s_{mutant}$ on the sensor chip, IMB-9C was injected at indicated concentrations. Binding of IMB-9C to $HR1s_{mutant}$ resulted in a concentration-dependent increase of the SPR signals expressed as resonance units (RU). The binding constant K_D was calculated from the changes in the SPR signal.

Please cite this article as: Zhang Jing et al., Yeast-two-hybrid based high-throughput screening to discover SARS-CoV-2 fusion inhibitors by targeting the HR1/HR2 interaction, Acta Pharmaceutica Sinica B, https://doi.org/10.1016/j.apsb.2025.06.029

Table 7 The kinetics data of SPR analysis.

Sample	K_{on} (1/Ms)	K_{off} (1/S)	K_D (mol/L)
HR1-A930G	7.80×10^3	9.86×10^{-2}	1.27×10^{-5}
HR1-I931G	3.74×10^2	1.01×10^{-1}	2.69×10^{-4}
HR1-K933G	2.62×10^4	3.76×10^{-1}	1.44×10^{-5}
HR1-T941G	8.16×10^3	4.37×10^{-1}	5.36×10^{-5}
HR1-L945G	1.67×10^3	5.38×10^{-1}	3.21×10^{-4}

Table 8 Drug-likeness of IMB-9C calculated by SwissADME.

Criteria	Recommendations	IMB-9C
MW[a]	<500	444.44
No. of HB donors[a]	<5	1
No. of HB acceptors[a]	<10	6
No. of rotatable bonds[a]	≤10	7
Consensus Log$P_{O/W}$[b]	2.25−4.75	2.40
Log$S$ (Ali)[c]	Insoluable < −10 < Poorly < −6 < Moderately < −4 < Soluable < −2 Very <0 < Highly	−5.38
GI absorption[d]	High	High
BBB permeant[d]		No
CYP enzymes inhibitors[d]	None	CYP2C19, CYP2C9, CYP3A4 inhibitor
Bioavailability score[e]	0 < Low <0.3 < Moderate <0.7 < High <1	0.55
Synthetic accessibility[f]	From 1 (very easy) to 10 (very difficult)	3.64

HB: Hydrogen bonding; Ali: A topological method to predict Water Solubility adapted from Ali et al.[50]; GI: Gastrointestinal; BBB: Blood−brain barrier; CYP: Cytochrome P450 proteins.
[a]Physicochemical properties.
[b]Lipophilicity.
[c]Water solubility.
[d]Pharmacokinetics.
[e]Druglikeness.
[f]Medicinal chemistry.

and 20% left within 40 min. While the content of IMB-9C in plasma did not reduce within 120 min, indicating its stability in plasma.

4. Discussion

COVID-19 caused by SARS-CoV-2 has led to a global pandemic. Despite the expeditious development of various vaccines and therapeutics, SARS-CoV-2 is likely to remain a significant public health concern in the foreseeable future for several reasons. First, variant viruses with escape mutations continue to emerge, which compromise the efficacy of vaccines[53]. Second, a portion of the population opt out of vaccination based on their religious beliefs, concerns of long-term side effects, or other reasons[54]. Third, the durability of COVID-19 vaccines is currently unknown[54]. As such, it is unpredictable when or whether herd immunity can be achieved. Besides, recent reports have suggested that some bat SARS-related coronaviruses (SARSr-CoVs) may cause novel CoVs diseases in the near future[55,56]. Therefore, antivirals are important complements of vaccines to[54] and the development of highly effective pan-CoV inhibitor-based prophylactics and therapeutics to combat both current and future outbreaks of infectious diseases caused by emerging and re-emerging CoVs.

Fusion inhibitors have demonstrated substantial promise for both prophylaxis and treatment of viral infections and are commonly used for treating HIV[57]. Fusion inhibition has also been found a useful strategy to inhibit SARS-CoV and MERS-CoV[40,58-61]. However, the comprehensive HTS of antiviral drugs targeting the HR1/HR2 complex is lacking. The Y2H system has been applied to the discovery of various interaction inhibitors[27,28,62,63]. It has many advantages, such as highly sensitivity to weak and transient interactions between proteins, requirement for little specialized equipment, low screening cost for HTS, verify PPIs point-by-point and so on. In this study, through the discovery of the positive compound IMB-9C, we confirmed for the first time the feasibility of the Y2H system in screening inhibitors targeting HR1 and HR2 interaction, providing a HTS method for inhibitors. In addition, the HR region is also a typical feature of class I enveloped viruses which is also found in murine hepatitis virus (MHV), SARS-CoV, influenza virus haemagglutinin (HA), human immunodeficiency virus (HIV), and mouse hepatitis virus[42,64]. Therefore, this Y2H method can not only be used for the screening of HR1/HR2 interaction inhibitors for coronaviruses, but it also has good reference significance for the discovery of antiviral drugs targeting host cell fusion of Type I enveloped virus. However, the Y2H system inevitably has its limitations, as the presence of cell walls may make it difficult for some compounds to enter the cell, resulting in false negatives. In the following research, further modification for Y2H system is needed, such as adopting AH109 cells with high permeability.

In silico design is an important strategy for drug design and screening. For HR1/HR2 interaction inhibitors, several peptide analogues were designed based on the structure of HR, such as peptide derived from HR2P[13,14,65,66], the coiled-coil structure of HR1 trimer[23,67], and a 5-helix construct based on the S2 6-HB structure but lacking one HR2 region[13,14,23,65-68]. However, the selection of sites for this virtual design is based on the previous experience from HIV inhibitors, and it is still unknown which sites can better exert inhibitory activity, which poses great difficulties for more accurate antiviral drug design and screening. In this study, we used IMB-9C as a probe to explore possible binding sites through virtual docking, and verified through amino acid mutations that A930, I931, K933, T941, and L945 are the key binding sites for IMB-9C and HR1. Meanwhile, as HR1 with mutations at I934, Q935, S937, L938, S939, S940, and T942 lost its interaction with HR2 in the H2Y system, indicating their key role in HR1−HR2 interaction. The elucidation of these key amino acid sites based on IMB-9C/HR1P interaction provides good clues for the design and screening of HR1 targeted drugs in the future.

Current fusion inhibition entities primarily encompass vaccines, peptides, antibodies, and small chemical molecules[69]. S2-based vaccines might present themselves as promising candidates. But the relatively low immunogenicity of S2-based antigens remains a significant hurdle to overcome[64]. Peptide-based fusion inhibitors hold an important position because of remarkable strengths such as high selectivity, less likelihood for drug resistance, safe to use, etc.[66,70,71] Recently, several S2 subunit-targeted

Please cite this article as: Zhang Jing et al., Yeast-two-hybrid based high-throughput screening to discover SARS-CoV-2 fusion inhibitors by targeting the HR1/HR2 interaction, Acta Pharmaceutica Sinica B, https://doi.org/10.1016/j.apsb.2025.06.029

neutralizing antibodies (nAbs) have been shown to exhibit cross-neutralizing activity against various coronaviruses [72-75]. However, as protein therapies, peptides and nAbs have weaknesses, including lack of oral availability [76], high production cost, relatively stringent storage condition, immunogenicity, short half-life, unstable under physiological conditions, poor solubility in water, etc.[77] Whereas, small molecules play an important role in drug development because of their unique advantages, including lower cost, mature production technology, higher adherence, higher stability leading to more ease of transportation and storage, as well as better pharmacokinetic behavior such as higher oral bioavailability and well-characterized *in vivo* safety, and etc.[64,76] There are already a few small-molecule compounds reported to protect against SARS-CoV-2 infection by blocking the HR1−HR2 bundle assembly[19,76,78-81], but their inhibitory activity against HR is primarily confirmed through molecular docking or protein−protein interaction. In comparison, IMB-9C stands out as the pioneering small molecule compound that exhibits confirmed affinity for both HR1 and HR2, with its precise mode of action thoroughly elucidated using mutant HR1. Although S2 is relatively conserved among different SARS-CoV2 Variants of Concern (VOCs), this dual binding characteristic retains the inhibitory potential of IMB-9C to HR mutations and decreases the likelihood of drug resistance, indicating its potential as an anti-COVID-19 drug.

Good antiviral activity, low cytotoxicity, certain metabolic stability *in vitro* and ADMET prediction all suggested that IMB-9C may have certain pharmacological properties, but further research on its antiviral activity *in vivo* and pharmacokinetic analysis is needed. The structural modification of IMB-9C is ongoing to enhance its antiviral activity and water solubility, thereby further refining its pharmacological attributes.

5. Conclusions

In this study, we have established a HTS method for SARS-CoV-2 HR1/HR2 interaction inhibitors based on Y2H system for the first time, and identified IMB-9C from 15,000 small molecule compounds. IMB-9C was able to compete with the intramolecular HR1/HR2 interaction, block fusion, and showed anti-SARS-CoV-2 activity *in vitro*, making it a favorable lead for designing of functionally improved inhibitors. Our results highlight the power of an *in vitro* approach to engineer potent and novel inhibitors targeting HR1/HR2 interaction. The method used in this manuscript can be applied to identify novel inhibitors related to viral host interaction beyond just a novel inhibitor, which will be quickly employed to identify compounds against other viruses.

Acknowledgments

This study was supported by CAMS Innovation Fund for Medical Sciences (CIFMS) (Nos. 2021-1-I2M-1-054, 2022-I2M-2-002, 2023-I2M-2-006, 2020-I2M-2-010, and 2021-I2M-1-070, China), National Natural Science Foundation of China (No. 81370087, China), Health and Medical Research Fund (HMRF) Commissioned Research on the Novel Coronavirus Disease (COVID1903010-Project 10, Hong Kong SAR, China), the PhD Research Startup Fund of Shanxi Medical University (XD2204, China), and the Provincial Doctoral Fund of Shanxi Medical University (SD2312, China). The author would like to thank Ms. Li−Li Niu at the CAS Research Platform for Protein Sciences for the support in mass spectrometry data collection and analysis (Institute of Biophysics, Chinese Academy of Sciences, Beijing, China).

Author contributions

Shuyi Si, Yan Li, Richard Yi Tsun Kao and Peng Gao conceived and designed the study, and revised the manuscript. Jing Zhang, Chao Liu, Wenwen Zhou, and Dongsheng Li performed the experiments. Peirong Wang and Peng Gao designed and performed antiviral assays. Baoqing You, Bingjie Su and Wenjing Shi analyzed the data. Tin Mong Timothy Yung and Peng Gao conducted molecular docking. Keyu Guo drew figures and tables. Jing Zhang prepared the manuscript. All authors have approved the final version of the manuscript.

Conflicts of interest

The authors declare no conflicts of interest.

Appendix A. Supporting information

Supporting information to this article can be found online at https://doi.org/10.1016/j.apsb.2025.06.029.

References

1. Zhou Z, Zhu YM, Chu M. Role of COVID-19 vaccines in SARS-CoV-2 variants. *Front Immunol* 2022;**13**:898192.
2. Hasan A, Paray BA, Hussain A, Qadir FA, Attar F, Aziz FM, et al. A review on the cleavage priming of the spike protein on coronavirus by angiotensin-converting enzyme-2 and furin. *J Biomol Struct Dyn* 2021;**39**:3025−33.
3. Hoffmann M, Kleine-Weber H, Schroeder S, Kruger N, Herrler T, Erichsen S, et al. SARS-CoV-2 cell entry depends on ACE2 and TMPRSS2 and is blocked by a clinically proven protease inhibitor. *Cell* 2020;**181**:271−280.e8.
4. Follis KE, York J, Nunberg JH. Furin cleavage of the SARS coronavirus spike glycoprotein enhances cell-cell fusion but does not affect virion entry. *Virology* 2006;**350**:358−69.
5. Braun E, Sauter D. Furin-mediated protein processing in infectious diseases and cancer. *Clin Transl Immunol* 2019;**8**:e1073.
6. Tsuji K, Baffour-Awuah Owusu K, Miura Y, Ishii T, Shinohara K, Kobayakawa T, et al. Dimerized fusion inhibitor peptides targeting the HR1−HR2 interaction of SARS-CoV-2. *RSC Adv* 2023;**13**:8779−93.
7. Xiao TS, Cai YF, Chen B. HIV-1 entry and membrane fusion inhibitors. *Viruses* 2021;**13**:735.
8. Steffen DL, Xu K, Nikolov DB, Broder CC. Henipavirus mediated membrane fusion, virus entry and targeted therapeutics. *Viruses* 2012;**4**:280−308.
9. Battini L, Fidalgo DM, Alvarez DE, Bollini M. Discovery of a potent and selective chikungunya virus envelope protein inhibitor through computer-aided drug design. *ACS Infect Dis* 2021;**7**:1503−18.
10. Steiner S, Kratzel A, Barut GT, Lang RM, Aguiar Moreira E, Thomann L, et al. SARS-CoV-2 biology and host interactions. *Nat Rev Microbiol* 2024;**22**:206−25.
11. Bestle D, Heindl MR, Limburg H, Van Lam T, Pilgram O, Moulton H, et al. TMPRSS2 and furin are both essential for proteolytic activation of SARS-CoV-2 in human airway cells. *Life Sci Alliance* 2020;**3**:e202000786.
12. Liang GD, Li Y, Li RJ, Ma YH, Na HY. Structure and function of the SARS-CoV-2 6-HB fusion core and peptide-based fusion inhibitors: a review. *Curr Med Chem* 2023;**32**:2524−46.

13. Xia S, Yan L, Xu W, Agrawal AS, Algaissi A, Tseng CK, et al. A pan-coronavirus fusion inhibitor targeting the HR1 domain of human coronavirus spike. *Sci Adv* 2019;**5**:eaav4580.
14. Xia S, Liu MQ, Wang C, Xu W, Lan QS, Feng SL, et al. Inhibition of SARS-CoV-2 (previously 2019-nCoV) infection by a highly potent pan-coronavirus fusion inhibitor targeting its spike protein that harbors a high capacity to mediate membrane fusion. *Cell Res* 2020;**30**:343−55.
15. Cannalire R, Stefanelli I, Cerchia C, Beccari AR, Pelliccia S, Summa V. SARS-CoV-2 entry inhibitors: small molecules and peptides targeting virus or host cells. *Int J Mol Sci* 2020;**21**:5707.
16. Wang XL, Sun LJ, Liu ZZ, Xing LX, Zhu Y, Xu W, et al. An engineered recombinant protein containing three structural domains in SARS-CoV-2 S2 protein has potential to act as a pan-human coronavirus entry inhibitor or vaccine antigen. *Emerg Microb Infect* 2023;**12**:2244084.
17. Lu Y, Shen F, He WQ, Li AQ, Li MH, Feng XL, et al. HR121 targeting HR2 domain in S2 subunit of spike protein can serve as a broad-spectrum SARS-CoV-2 inhibitor *via* intranasal administration. *Acta Pharm Sin B* 2023;**13**:3339−51.
18. Outlaw VK, Bovier FT, Mears MC, Cajimat MN, Zhu Y, Lin MJ, et al. Inhibition of coronavirus entry *in vitro* and *ex vivo* by a lipid-conjugated peptide derived from the SARS-CoV-2 spike glycoprotein HRC domain. *mBio* 2020;**11**:e01935-20.
19. Yang C, Pan XY, Huang Y, Cheng C, Xu XF, Wu Y, et al. Drug repurposing of Itraconazole and Estradiol Benzoate against COVID-19 by blocking SARS-CoV-2 spike protein-mediated membrane fusion. *Adv Ther* 2021;**4**:2000224.
20. Ling RS, Dai YR, Huang BX, Huang WJ, Yu JF, Lu XF, et al. *In silico* design of antiviral peptides targeting the spike protein of SARS-CoV-2. *Peptides* 2020;**130**:170328.
21. Yin XJ, Chen LT, Yuan SW, Liu L, Gao ZZ. A robust high-throughput fluorescent polarization assay for the evaluation and screening of SARS-CoV-2 fusion inhibitors. *Bioorg Chem* 2021;**116**:105362.
22. Yarovaya OI, Shcherbakov DN, Borisevich SS, Sokolova AS, Gureev MA, Khamitov EM, et al. Borneol ester derivatives as entry inhibitors of a wide spectrum of SARS-CoV-2 viruses. *Viruses* 2022;**14**:1295.
23. Cano-Munoz M, Polo-Megias D, Camara-Artigas A, Gavira JA, Lopez-Rodriguez MJ, Laumond G, et al. Novel chimeric proteins mimicking SARS-CoV-2 spike epitopes with broad inhibitory activity. *Int J Biol Macromol* 2022;**222**:2467−78.
24. Gentile D, Coco A, Patamia V, Zagni C, Floresta G, Rescifina A. Targeting the SARS-CoV-2 HR1 with small molecules as inhibitors of the fusion process. *Int J Mol Sci* 2022;**23**:10067.
25. Yuan SF, Yin X, Meng XZ, Chan JF, Ye ZW, Riva L, et al. Clofazimine broadly inhibits coronaviruses including SARS-CoV-2. *Nature* 2021;**593**:418−23.
26. Chen Q, Wei TY. Membrane and nuclear yeast two-hybrid systems. *Methods Mol Biol* 2022;**2400**:93−104.
27. Lin Y, Li Y, Zhu YJ, Zhang J, Li YZ, Liu X, et al. Identification of antituberculosis agents that target ribosomal protein interactions using a yeast two-hybrid system. *Proc Natl Acad Sci U S A* 2012;**109**:17412−7.
28. Li Y, Zhu XH, Zhang J, Lin Y, You XF, Chen MH, et al. Identification of a compound that inhibits the growth of gram-negative bacteria by blocking BamA−BamD interaction. *Front Microbiol* 2020;**11**:1252.
29. Wen K, Cai JP, Fan XD, Zhang XJ, Luo CT, Tang KM, et al. Broad-spectrum humanized monoclonal neutralizing antibody against SARS-CoV-2 variants, including the Omicron variant. *Front Cell Infect Microbiol* 2023;**13**:1213806.
30. Chu H, Chan JF, Yuen TT, Shuai HP, Yuan SF, Wang YX, et al. Comparative tropism, replication kinetics, and cell damage profiling of SARS-CoV-2 and SARS-CoV with implications for clinical manifestations, transmissibility, and laboratory studies of COVID-19: an observational study. *Lancet Microbe* 2020;**1**:e14−23.
31. Xia S, Lan QS, Pu J, Wang C, Liu ZZ, Xu W, et al. Potent MERS-CoV fusion inhibitory peptides identified from HR2 domain in spike protein of bat coronavirus HKU4. *Viruses* 2019;**11**:56.
32. Chen YL, Wu Y, Chen SY, Zhan QP, Wu DZ, Yang C, et al. Sertraline is an effective SARS-CoV-2 entry inhibitor targeting the spike protein. *J Virol* 2022;**96**:e0124522.
33. Xing LX, Xu XF, Xu W, Liu ZZ, Shen X, Zhou J, et al. A five-helix-based SARS-CoV-2 fusion inhibitor targeting heptad repeat 2 domain against SARS-CoV-2 and its variants of concern. *Viruses* 2022;**14**:597.
34. Trott O, Olson AJ. AutoDock Vina: improving the speed and accuracy of docking with a new scoring function, efficient optimization, and multithreading. *J Comput Chem* 2010;**31**:455−61.
35. Pettersen EF, Goddard TD, Huang CC, Couch GS, Greenblatt DM, Meng EC, et al. UCSF Chimera–a visualization system for exploratory research and analysis. *J Comput Chem* 2004;**25**:1605−12.
36. Wallace AC, Laskowski RA, Thornton JM. LIGPLOT: a program to generate schematic diagrams of protein-ligand interactions. *Protein Eng* 1995;**8**:127−34.
37. Daina A, Michielin O, Zoete V. SwissADME: a free web tool to evaluate pharmacokinetics, drug-likeness and medicinal chemistry friendliness of small molecules. *Sci Rep* 2017;**7**:42717.
38. Fuloria S, Mehta J, Chandel A, Sekar M, Rani N, Begum MY, et al. A comprehensive review on the therapeutic potential of curcuma longa linn. in relation to its major active constituent curcumin. *Front Pharmacol* 2022;**13**:820806.
39. Sardar H. Drug like potential of daidzein using SwissADME prediction: *in silico* approaches. *PHYTONutrients* 2023;**2**:2−8.
40. Lu L, Liu Q, Zhu Y, Chan KH, Qin LL, Li Y, et al. Structure-based discovery of Middle East respiratory syndrome coronavirus fusion inhibitor. *Nat Commun* 2014;**5**:3067.
41. Leslie GJ, Wang JB, Richardson MW, Haggarty BS, Hua KL, Duong J, et al. Potent and broad inhibition of HIV-1 by a peptide from the gp41 heptad repeat-2 domain conjugated to the CXCR4 amino terminus. *PLoS Pathog* 2016;**12**:e1005983.
42. Jackson CB, Farzan M, Chen B, Choe H. Mechanisms of SARS-CoV-2 entry into cells. *Nat Rev Mol Cell Biol* 2022;**23**:3−20.
43. Zhao MM, Zhu Y, Zhang L, Zhong GX, Tai LH, Liu S, et al. Novel cleavage sites identified in SARS-CoV-2 spike protein reveal mechanism for cathepsin L-facilitated viral infection and treatment strategies. *Cell Discov* 2022;**8**:53.
44. Chang MC, Chen JH, Lee HN, Chen SY, Zhong BH, Dhingra K, et al. Inducing cathepsin L expression/production, lysosomal activation, and autophagy of human dental pulp cells by dentin bonding agents, camphorquinone and BisGMA and the related mechanisms. *Biomater Adv* 2023;**145**:213253.
45. Aiewsakun P, Phumiphanjarphak W, Ludowyke N, Purwono PB, Manopwisedjaroen S, Srisaowakarn C, et al. Systematic exploration of SARS-CoV-2 adaptation to Vero E6, Vero E6/TMPRSS2, and Calu-3 cells. *Genome Biol Evol* 2023;**15**:evad035.
46. Park JE, Li K, Barlan A, Fehr AR, Perlman S, Mccray Jr PB, et al. Proteolytic processing of Middle East respiratory syndrome coronavirus spikes expands virus tropism. *Proc Natl Acad Sci U S A* 2016;**113**:12262−7.
47. Clark DE, Grootenhuis PD. Progress in computational methods for the prediction of ADMET properties. *Curr Opin Drug Discov Dev* 2002;**5**:382−90.
48. Modi S. Computational approaches to the understanding of ADMET properties and problems. *Drug Discov Today* 2003;**8**:621−3.
49. Van De Waterbeemd H, Gifford E. ADMET *in silico* modelling: towards prediction paradise?. *Nat Rev Drug Discov* 2003;**2**:192−204.
50. Ali J, Camilleri P, Brown MB, Hutt AJ, Kirton SB. Revisiting the general solubility equation: *in silico* prediction of aqueous solubility incorporating the effect of topographical polar surface area. *J Chem Inf Model* 2012;**52**:420−8.
51. Masimirembwa CM, Bredberg U, Andersson TB. Metabolic stability for drug discovery and development: pharmacokinetic and biochemical challenges. *Clin Pharmacokinet* 2003;**42**:515−28.

Please cite this article as: Zhang Jing et al., Yeast-two-hybrid based high-throughput screening to discover SARS-CoV-2 fusion inhibitors by targeting the HR1/HR2 interaction, Acta Pharmaceutica Sinica B, https://doi.org/10.1016/j.apsb.2025.06.029

52. Kerns EH, Di L. Pharmaceutical profiling in drug discovery. *Drug Discov Today* 2003;**8**:316−23.
53. Harvey WT, Carabelli AM, Jackson B, Gupta RK, Thomson EC, Harrison EM, et al. SARS-CoV-2 variants, spike mutations and immune escape. *Nat Rev Microbiol* 2021;**19**:409−24.
54. Ma CL, Xia ZL, Sacco MD, Hu YM, Townsend JA, Meng XZ, et al. Discovery of di- and trihaloacetamides as covalent SARS-CoV-2 main protease inhibitors with high target specificity. *J Am Chem Soc* 2021;**143**:20697−709.
55. Yao HP, Song YT, Chen Y, Wu NP, Xu JL, Sun CJ, et al. Molecular architecture of the SARS-CoV-2 virus. *Cell* 2020;**183**:730−8 e713.
56. Shi R, Shan C, Duan XM, Chen ZH, Liu PP, Song JW, et al. A human neutralizing antibody targets the receptor-binding site of SARS-CoV-2. *Nature* 2020;**584**:120−4.
57. Eggink D, Berkhout B, Sanders RW. Inhibition of HIV-1 by fusion inhibitors. *Curr Pharm Des* 2010;**16**:3716−28.
58. Liu SW, Xiao GF, Chen YB, He YX, Niu JK, Escalante CR, et al. Interaction between heptad repeat 1 and 2 regions in spike protein of SARS-associated coronavirus: implications for virus fusogenic mechanism and identification of fusion inhibitors. *Lancet* 2004;**363**:938−47.
59. Chu LH, Chan SH, Tsai SN, Wang Y, Cheng CH, Wong KB, et al. Fusion core structure of the severe acute respiratory syndrome coronavirus (SARS-CoV): in search of potent SARS-CoV entry inhibitors. *J Cell Biochem* 2008;**104**:2335−47.
60. Liu IJ, Kao CL, Hsieh SC, Wey MT, Kan LS, Wang WK. Identification of a minimal peptide derived from heptad repeat (HR) 2 of spike protein of SARS-CoV and combination of HR1-derived peptides as fusion inhibitors. *Antivir Res* 2009;**81**:82−7.
61. Sainz B Jr, Mossel EC, Gallaher WR, Wimley WC, Peters CJ, Wilson RB, et al. Inhibition of severe acute respiratory syndrome-associated coronavirus (SARS-CoV) infectivity by peptides analogous to the viral spike protein. *Virus Res* 2006;**120**:146−55.
62. Khazak V, Golemis EA, Weber L. Development of a yeast two-hybrid screen for selection of human Ras-Raf protein interaction inhibitors. *Methods Mol Biol* 2005;**310**:253−71.
63. Wang WW, Liu C, Zhu NY, Lin Y, Jiang JD, Wang YC, et al. Identification of anti-gram-negative bacteria agents targeting the interaction between ribosomal proteins L12 and L10. *Acta Pharm Sin B* 2018;**8**:772−83.
64. Guo LY, Lin S, Chen ZM, Cao Y, He B, Lu GW. Targetable elements in SARS-CoV-2 S2 subunit for the design of pan-coronavirus fusion inhibitors and vaccines. *Signal Transduct Targeted Ther* 2023;**8**:197.
65. Bosch BJ, Martina BE, Van Der Zee R, Lepault J, Haijema BJ, Versluis C, et al. Severe acute respiratory syndrome coronavirus (SARS-CoV) infection inhibition using spike protein heptad repeat-derived peptides. *Proc Natl Acad Sci U S A* 2004;**101**:8455−60.
66. Schutz D, Ruiz-Blanco YB, Munch J, Kirchhoff F, Sanchez-Garcia E, Muller JA. Peptide and peptide-based inhibitors of SARS-CoV-2 entry. *Adv Drug Deliv Rev* 2020;**167**:47−65.
67. Wang C, Xia S, Wang XL, Li Y, Wang H, Xiang R, et al. Supercoiling structure-based design of a trimeric coiled-coil peptide with high potency against HIV-1 and Human beta-coronavirus infection. *J Med Chem* 2022;**65**:2809−19.
68. Miura K. An overview of current methods to confirm protein−protein interactions. *Protein Pept Lett* 2018;**25**:728−33.
69. Na HY, Liang GD, Lai WQ. Isopeptide bond bundling superhelix for designing antivirals against enveloped viruses with class I fusion proteins: a review. *Curr Pharm Biotechnol* 2023;**24**:1774−83.
70. Panchal D, Kataria J, Patel K, Crowe K, Pai V, Azizogli AR, et al. Peptide-based inhibitors for SARS-CoV-2 and SARS-CoV. *Adv Ther* 2021;**4**:2100104.
71. Zhou J, Xu W, Liu ZZ, Wang C, Xia S, Lan QS, et al. A highly potent and stable pan-coronavirus fusion inhibitor as a candidate prophylactic and therapeutic for COVID-19 and other coronavirus diseases. *Acta Pharm Sin B* 2022;**12**:1652−61.
72. Dacon C, Tucker C, Peng L, Lee CD, Lin TH, Yuan M, et al. Broadly neutralizing antibodies target the coronavirus fusion peptide. *Science* 2022;**377**:728−35.
73. Zhou PP, Song G, Liu HJ, Yuan M, He WT, Beutler N, et al. Broadly neutralizing anti-S2 antibodies protect against all three human beta-coronaviruses that cause deadly disease. *Immunity* 2023;**56**:669−686.e667.
74. Li TF, Kan QQ, Ge JY, Wan ZM, Yuan MQ, Huang Y, et al. A novel linear and broadly neutralizing peptide in the SARS-CoV-2 S2 protein for universal vaccine development. *Cell Mol Immunol* 2021;**18**:2563−5.
75. Shi W, Wang LS, Zhou TQ, Sastry M, Yang ES, Zhang Y, et al. Vaccine-elicited murine antibody WS6 neutralizes diverse beta-coronaviruses by recognizing a helical stem supersite of vulnerability. *Structure* 2022;**30**:1233−1244.e1237.
76. Jiao FK, Andrianov AM, Wang LJ, Furs KV, Gonchar AV, Wang Q, et al. Repurposing Navitoclax to block SARS-CoV-2 fusion and entry by targeting heptapeptide repeat sequence 1 in S2 protein. *J Med Virol* 2023;**95**:e29145.
77. Li DS, You BQ, Guo KY, Zhou WW, Li Y, Wang CY, et al. Establishment of a yeast two-hybrid-based high-throughput screening model for selection of SARS-CoV-2 spike-ACE2 interaction inhibitors. *Int J Mol Sci* 2025;**26**:678.
78. Pu J, He XY, Xu W, Wang C, Lan QS, Hua C, et al. The analogs of furanyl methylidene rhodanine exhibit broad-spectrum inhibitory and inactivating activities against enveloped viruses, including SARS-CoV-2 and its variants. *Viruses* 2022;**14**:489.
79. Yang C, Pan XY, Xu XF, Cheng C, Huang Y, Li L, et al. Salvianolic acid C potently inhibits SARS-CoV-2 infection by blocking the formation of six-helix bundle core of spike protein. *Signal Transduct Targeted Ther* 2020;**5**:220.
80. Mondal S, Karmakar A, Mallick T, Begum NA. Exploring the efficacy of naturally occurring biflavone based antioxidants towards the inhibition of the SARS-CoV-2 spike glycoprotein mediated membrane fusion. *Virology* 2021;**556**:133−9.
81. Jana ID, Bhattacharya P, Mayilsamy K, Banerjee S, Bhattacharje G, Das S, et al. Targeting an evolutionarily conserved "E-L-L" motif in spike protein to identify a small molecule fusion inhibitor against SARS-CoV-2. *PNAS Nexus* 2022;**1**:pgac198.

Please cite this article as: Zhang Jing et al., Yeast-two-hybrid based high-throughput screening to discover SARS-CoV-2 fusion inhibitors by targeting the HR1/HR2 interaction, Acta Pharmaceutica Sinica B, https://doi.org/10.1016/j.apsb.2025.06.029